Development of an Advanced Vaneless Inlet Particle Separator for Helicopter Engines

B. V. R. Vittal,* D. L. Tipton,† and W. A. Bennett‡
General Motors Corporation, Indianapolis, Indiana

Design and development of an advanced integral engine particle separator are presented to meet the challenging operational requirements of helicopter engines of the future. The vaneless, low-weight, high-efficiency separator makes it possible to achieve new levels of engine reliability, durability, and life cycle costs. This paper presents the analytical methods developed, the design process, and the extensive experimental validation of the design.

Nomenclature

A	= area of flow
C_d	= coefficient of drag of the particle
C_f	= skin-friction coefficient
d_h, D	= hydraulic and particle diameters, respectively
dp_t	= total pressure loss
e_N, e_T	= normal and tangential particle restitution ratios, respectively
IPS	= inlet particle separator
M	= Mach number
P	= pressure
Pt	= total pressure
t	= time
V_N, V_T	= normal and tangential components of particle velocity
V_x, V_r, V_θ	= flow velocity in axial, radial, and tangential directions
x, r, θ	= axial, radial, and tangential coordinates
Z	= shape factor
β_1	= particle impingement angle
γ	= ratio of specific heats
ρ, ρ_p	= gas and particle density, respectively

Introduction

INLET particle separators (IPS) are vital to the successful operation of helicopter gas turbine engines in dust or sand environments where ingestion of contaminated air can reduce engine life and drastically affect its performance. The limited operating life of unprotected engines gives rise to expensive overhaul cost. This problem becomes more serious for advanced technology compressors with high specific flows, which are more prone to erosion damage due to increased tip speed, reduced blade thickness, and close running clearances. The design requirements for gas turbine air cleaners are therefore becoming more challenging.

Among the air-cleaning systems that have been used on helicopters are barrier filters, vortex tube panels, and inertial separators. Barrier filters have not proved successful due to the necessity of frequent filter cleaning or replacement. The barrier filters were also prone to dislodging particles from the filter into the engine due to aircraft vibration. The vortex tube panel provides high separation efficiency but requires a relatively large frontal area and installed volume. The integral inertial separator has provided a good compromise for engine protection from sand, dust, and foreign objects while maintaining compactness and convenient anti-icing capability. The two basic types of inertial separators currently in use are the swirl and vaneless configurations. The swirl-type system uses a vane row to introduce a swirl to the contaminated inlet flow. The resulting centrifugal force field causes the heavier sand particles to migrate to the outer wall and into the scavenge duct. The vaneless separator is considerably simpler. It has less core pressure drop, weight, and cost, and fewer deicing power requirements, as compared to the swirl configuration. Particle separation is achieved by contouring the inner and outer walls to achieve rebound characteristics that direct the particles to the scavenge duct. Particle separation is further enhanced by introducing a linear momentum to the particles as they flow over the hump of the centerbody. The inertia of the particles then carries them into the scavenge duct. A swirless or vaneless inertial separator is especially suitable for engines in the 5-10-lb/s mass flow range. This paper presents the analytical methods developed for vaned and vaneless particle separators, the design process, and the extensive experimental validation of the design of a vaneless separator.

IPS Design System/Process

A design system for inertial particle separators, which is based on a building block of advanced analytical techniques for through-flow and particle trajectory analysis, is shown in Fig. 1.

Through-Flow Analysis

A through-flow analysis computer code VFLOW has been developed[1] using a body-fitted grid system for detailed flow analysis around the splitter, as well as hub and shroud surfaces. The code uses a stream-function formulation for arbitrary coordinate systems. The stream-function approach is a natural choice because it allows the specification of the flow split between the core and scavenge ducts. Fabian and Oates[2] and Hamed[3] used the stream-function approach, but they treated each duct independently by estimating the dividing streamline upstream of the splitter. The analysis used here simultaneously calculates the flow in the inlet core and scavenge ducts. The governing equations for axisymmetric inviscid rotational flow were transformed to arbitrary curvilinear coordinates and applied to a body-fitted coordinate system.

The body-fitted grid provides accurate resolution of the high-velocity flowfield around the splitter. The method has

Presented as Paper 85-1277 at the AIAA/SAE/ASME/ASEE 21st Joint Propulsion Conference, Monterey, CA, July 8-10, 1985; received July 22, 1985; revision received March 15, 1986.

*Development Engineer, Compressor Aerodynamics, Allison Gas Turbine Division. Member AIAA.
†Supervisor, Flow Systems, Allison Gas Turbine Division.
‡Senior Experimental Engineer, Allison Gas Turbine Division.

been verified by comparing the analytical results with experimental data. Within the limits of the inviscid compressible rotational flow approximation, excellent correlation between the numerical solutions and the experimental data have been obtained.

For separators with swirl vanes, the NASA MERIDL[4] program was modified and integrated with the design system to provide a detailed intravane flow analysis, including body forces. This addition provides vane profile determination and improved accuracy for three-dimensional particle trajectory calculations, including particle impact on the vanes.

For more complex cases, intrablade three-dimensional flow solutions can be obtained using the analysis of Denton,[5] which computes three-dimensional inviscid flow using a finite-volume time-marching scheme.

Wall Boundary-Layer and Pressure-Loss Analysis

Boundary-layer growth on hub, tip, and splitter surfaces of the separator has a predominant effect on the total pressure loss. Any separation of these boundary layers may drastically affect the flow into the compressor, which consequently may affect the surge margin of the compressor. A compressible boundary-layer code, initially developed by McNally,[6] has been modified and adapted to the IPS design system.

A computer code to calculate the total pressure loss in IPS, using the surface boundary-layer data, is also part of the design system. Considering a control volume in the duct and making a force balance, a simple expression for the total pressure loss is given by [7]

$$\frac{dp_t}{P_t} = -\frac{\gamma M^2}{2}\left\{4Cf\frac{dx}{d_h} + \frac{dl}{\frac{1}{2}\gamma PAM^2}\right\}$$

where dl is the internal drag representing the boundary-layer momentum deficit. Knowing the boundary-layer data, the total pressure loss is calculated by numerically integrating this equation using the finite-difference method.

Particle Trajectory Analysis

The backbone of the IPS design system is the advanced computer code VTRAJ developed to calculate the separation efficiency for a wide range of particle sizes by simulating the particle trajectories in a swirling flowfield. The particle dynamics of a gas-solid suspension are determined by the gas-particle interaction and particle-boundary impacts. The trajectory of a particle in a moving fluid is governed by the vector balance of its rate of change of momentum and the external forces. The external force field, as established by the primary airflow, is defined by the through-flow analytical code. The three-dimensional Lagrangian equations of motion, including centrifugal and coriolis acceleration terms, are given by[3]

$$\frac{d^2x}{dt^2} = G\left(V_x - \frac{dx}{dt}\right)$$

$$\frac{d^2r}{dt^2} = G\left(V_r - \frac{dr}{dt}\right) + r\left(\frac{d\theta}{dt}\right)^2$$

$$\frac{d^2\theta}{dt^2} = \frac{G}{r}\left(V_\theta - r\frac{d\theta}{dt}\right) - \frac{2dr}{rdt}\frac{d\theta}{dt}$$

where

$$G = \frac{\pi C_d}{8DZ}\frac{\rho}{\rho_p}V_{\text{rel}}$$

and x, r, and θ define the particle location in axial, radial, and tangential directions respectively. The coefficient of drag of the particle C_d depends on the Reynolds number, which is based on the relative velocity between the particle and fluid. Empirical correlations[8] for a wide range of particle Reynolds numbers are used for drag calculation. The equations of motion are integrated numerically to calculate the particle trajectories. Particles impacting on the surfaces change their velocities both in magnitude and direction. The following empirical relations for the rebound to impact restitution ratios are used in the trajectory calculations[9]:

$$e_N = V_{N_2}/V_{N_1} = 1.0 - 0.0211\,\beta_1 + 0.0002278\,\beta_1^2 - 0.000000876\beta_1^3$$

$$e_T = V_{T_2}/V_{T_1} = 0.953 - 0.000446\,\beta_1^2 + 0.00000648\,\beta_1^3$$

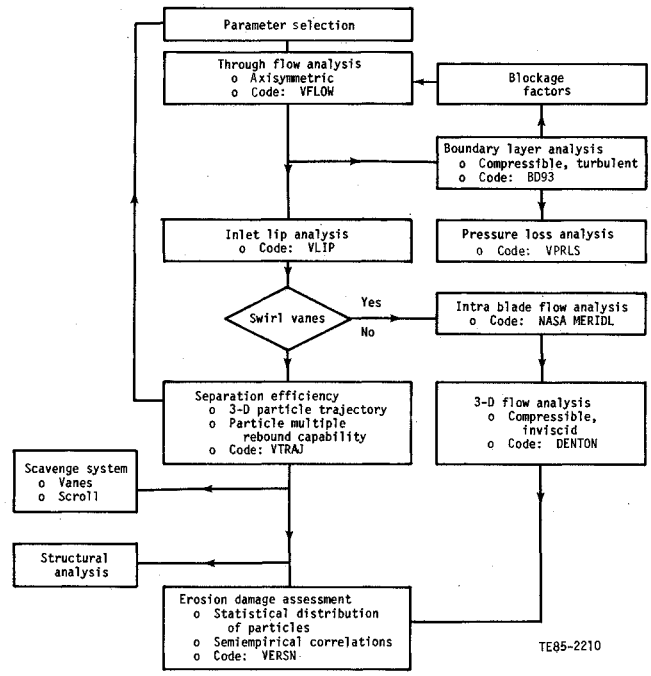

Fig. 1 IPS design system/process.

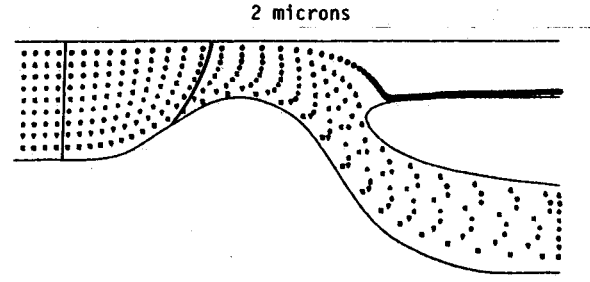

Fig. 2 Representative particle trajectories (without swirl vane impact) for 2-μ-diam particles.

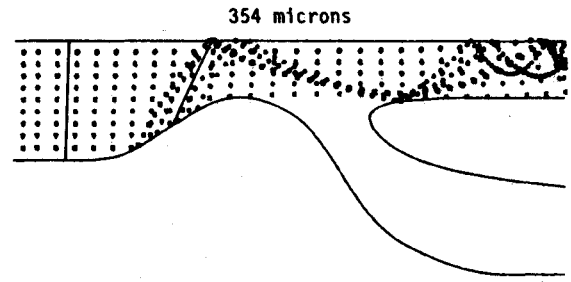

Fig. 3 Representative particles trajectories (without swirl vane impact) for 354-μ-diam particles.

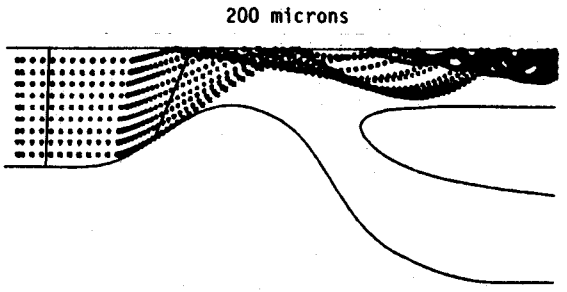

Fig. 4 Typical particle trajectories (with swirl vane impact) for 200-μ-diam particles.

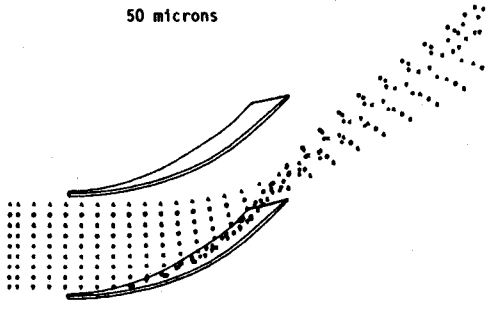

Fig. 5 Typical particle trajectories in the blade-to-blade plane for 50-μ-diam particles.

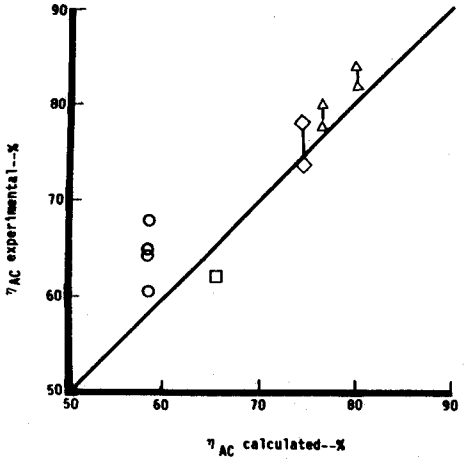

Fig. 6 Comparison of analytical and experimental separation efficiency resuls for AC coarse dust.

The particle impacts on the vanes (if present), splitter, and inner and outer annuli are accurately represented in the particle trajectory calculations. Provision is made for the automatic computation of the separation efficiency as a function of both particle size and specified sand composition like C-spec (0-10000 μ) sand and AC coarse dust (0-200μ). Separation efficiency is defined as the ratio of the weight of sand or dust collected in the scavenge to that ingested at the inlet. Plot procedures are incorporated into the code to give trajectory plots showing rebound, acceleration, and deceleration of the particles for different particle sizes. Figures 2 and 3 show representative particle trajectories in a swirl vaned separator for 2- and 354-μ-diam particles. These particles are moving between the inlet swirl vanes without impacting on them. Figure 4 shows the trajectories of 200-μ-diam particles, with the particles impacting the vanes. The particles are centrifuged out in the radial plane, after hitting the swirl vanes, due to the imposed tangential velocity. This activity can be seen in Fig. 5, where representative trajectories are plotted for 50-μ-diam particles in the blade-to-blade plane.

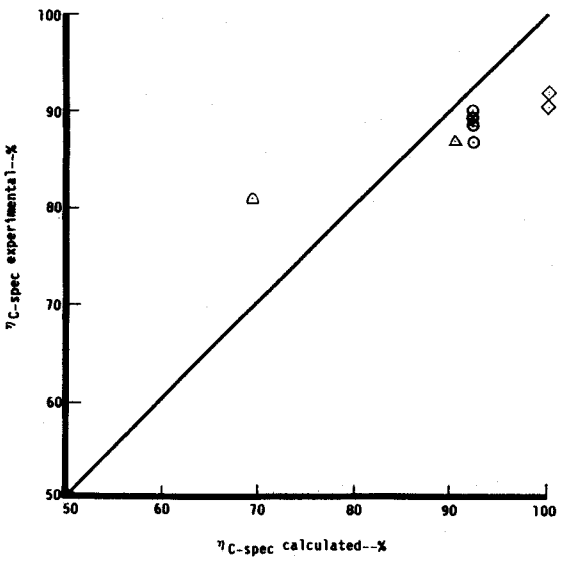

Fig. 7 Comparison of analytical and experimental separation efficiency results for C-spec sand.

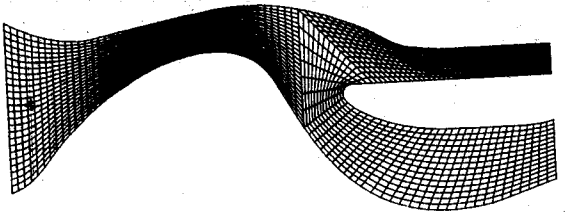

Fig. 8 Aerodynamic flow path of the advanced vaneless separator with the solution grid.

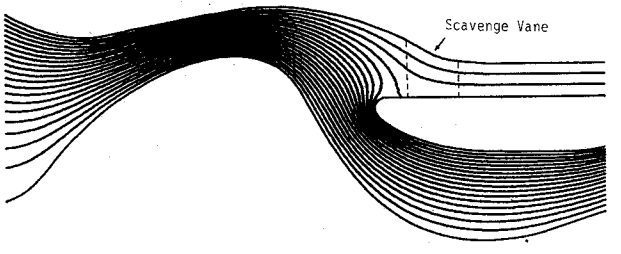

Fig. 9 Separator flow streamline pattern.

The design and analysis system has been used to analyze existing separators, and the results have been compared with test data, as shown in Figs. 6 and 7. The comparison for AC coarse dust is good.

The experimental values of separation efficiency are lower than predicted for C-spec sand. This difference may be due to the shattering of the particles into smaller sizes due to impact and/or due to the statistical nature of the particle rebound phenomenon. These aspects are currently being studied.

In the final phase of the design iteration, the erosion damage assessment program module is used to calculate the erosion pattern on the swirl vanes as well as the hub, shroud, and splitter surfaces of the separator.

Design of Vaneless Separator

The advanced inertial inlet particle separators are required to achieve maximum separation efficiency for a wide range of particle sizes, with minimum total pressure loss, low scavenge airflow requirement, and minimal or no distortion to the air entering the compressor. In addition, IPS needs to be compact to reduce the frontal area and weight. These requirements are sometimes in conflict with each other. The separator was

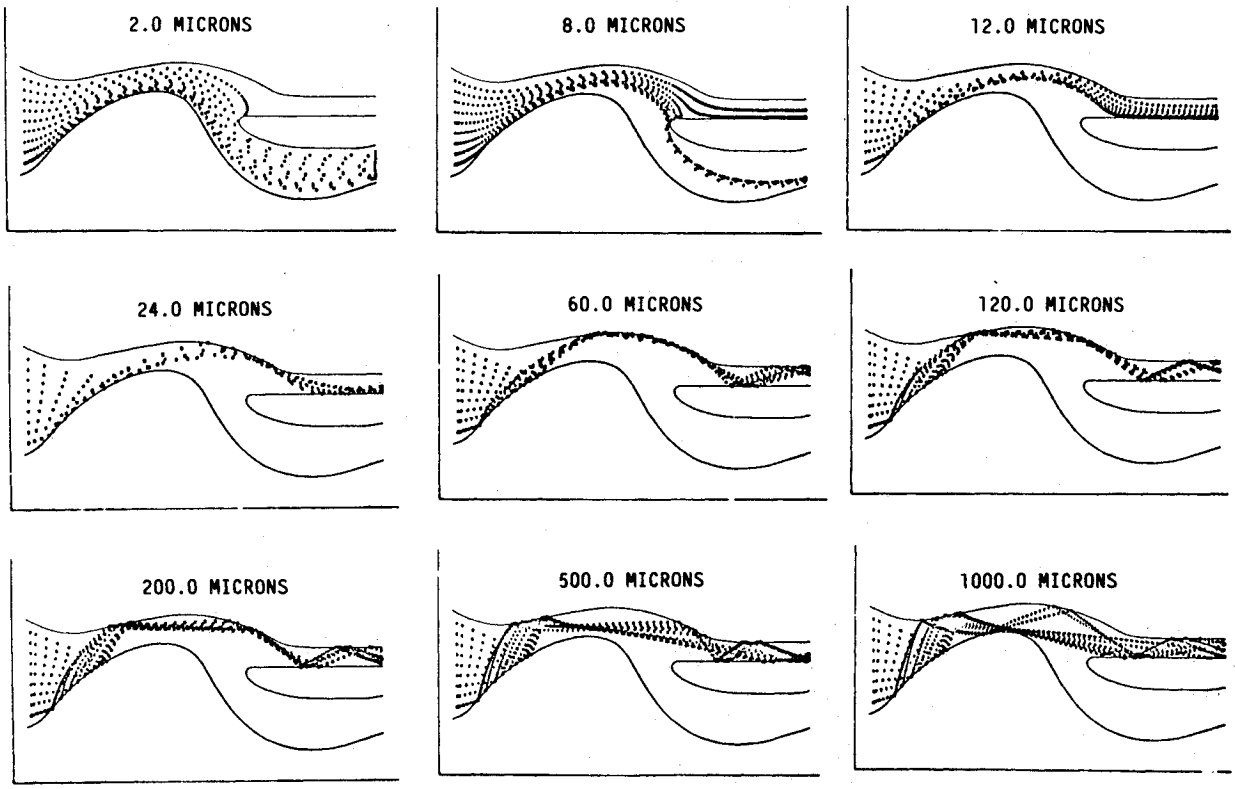

Fig. 10 Particle trajectories for advanced inlet particle separator.

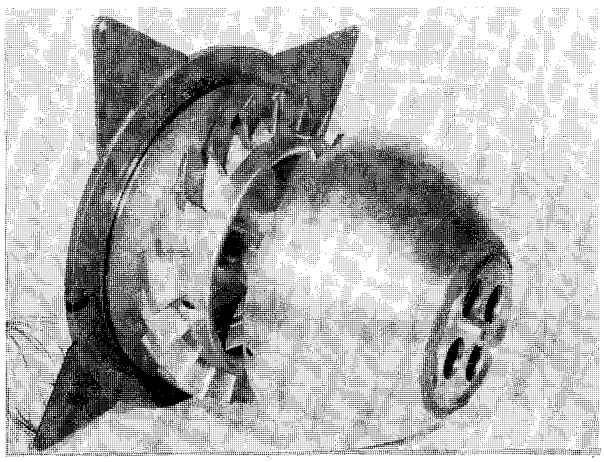

Fig. 11 Inlet particle separator hardware showing centerbody ramp and scavenge vanes.

designed for a total mass flow of 6.0 lb/s, with 15% of it going to scavenge. The various dimensions of the separator were carefully selected after a number of iterations with various tradeoff studies. Figure 8 shows the aerodynamic flow path of IPS with the solution grid imposed on it. The inlet hub and shroud were selected to provide low inlet Mach numbers to minimize entry loss. The splitter is hidden from the inlet by the large hub ramp to obtain high separation efficiency. The axial location of the splitter has been selected to achieve high separation efficiency while maintaining acceptable surface velocity around the flow splitter. The selected scavenge area balances the need for a large trajectory target area against the need for a reduced area to maintain linear momentum of the particulate flow. The selected area also provides low Mach numbers entering the scavenge vanes to minimize erosion and aerodynamic loss. Scavenge vanes have been incorporated to circumferentially direct the flow and the sand to the scroll inlet with minimum loss. A scroll-type scavenge flow collector was used to scavenge the particles. The flow streamline pattern is shown in Fig. 9. Figure 10 illustrates the particle trajectories of different-sized particles in the separator. The separator hardware, illustrated in Fig. 11, shows the centerbody ramp and scavenge vanes.

Test Program

Development of a successful inlet particle separator requires full-scale testing. The pronounced effect of flow size on the effectiveness of separators prohibits the use of subscale devices to acquire accurate separation efficiency measurements. Scaled models, however, may be used for aerodynamic measurement tests.The advanced vaneless separator was taken through a series of tests using full-scale models for both separation and aerodynamic measurements. The test program is illustrated in Fig. 12.

Aerodynamic Measurements

A test rig was designed with enough flexibility to allow for detailed measurements of the flowfields in all critical channels. Steam ejectors were used to provide the necessary suction for primary and scavenge flow lines. Additional wall static taps were provided for those areas of the flowfield in which boundary-layer separation or reattachment was suspected. The entire flowfield at the core exit was mapped by means of a circumferential/radial traverse mechanism. A close-coupled shrouded probe, a high-response hot-film probe, and a subminiature high-response dynamic pressure probe were mounted at the core exit. The shrouded probe and the hot-film probe were mounted to a rack-and-pinion gear arrangement, which under computer control accurately mapped the velocity and total pressure fields at the core exit. A 1600-point survey was taken at the core exit to determine the total pressure loss.

Sand Ingestion Tests

The sand ingestion system included a hopper with secondary airflow supply to inject the sand particles. To control the sand flow rate, the air pressure of the delivery line, the pressure in

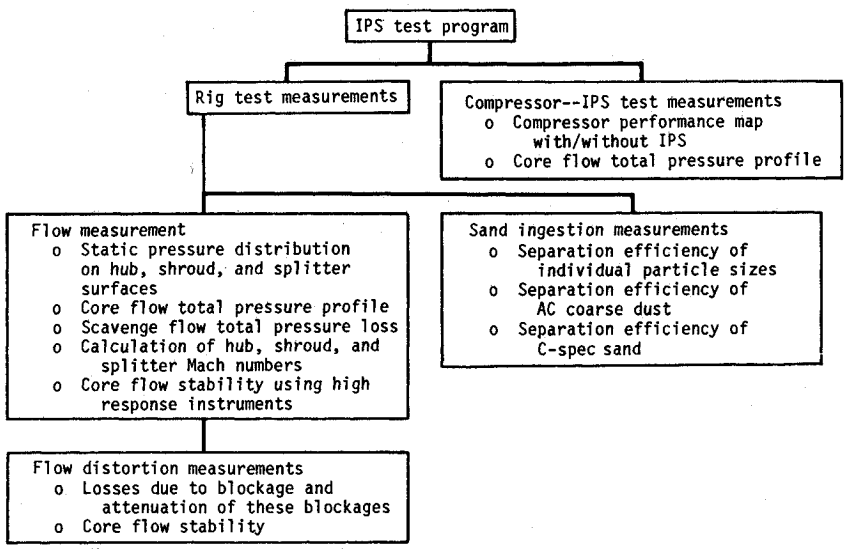

Fig. 12 Test Program.

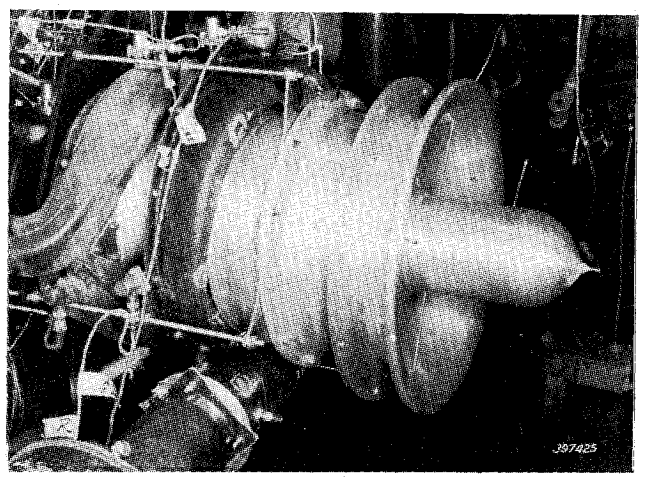

a) Sand ingestion rig.

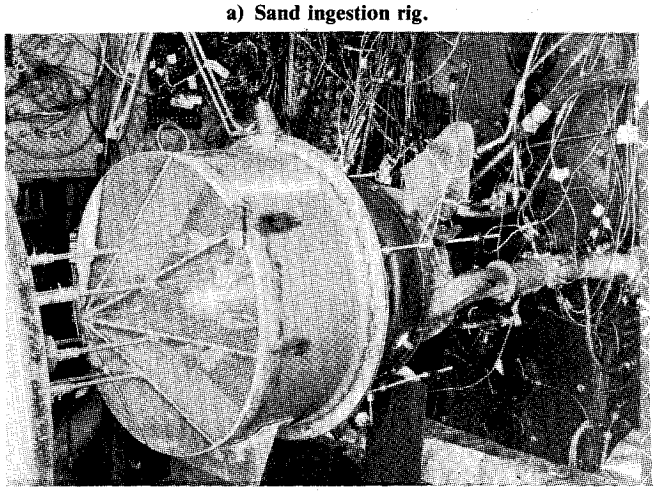

b) Aerodynamic rig.

Fig. 13 IPS test setup.

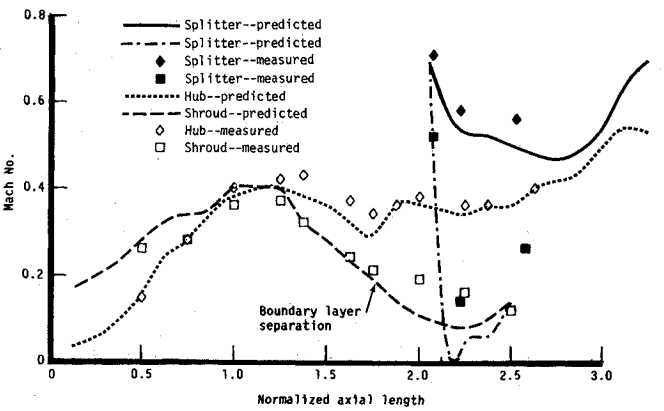

Fig. 14 Comparison of analytical and experimental Mach number distribution on hub, shroud, and splitter surfaces.

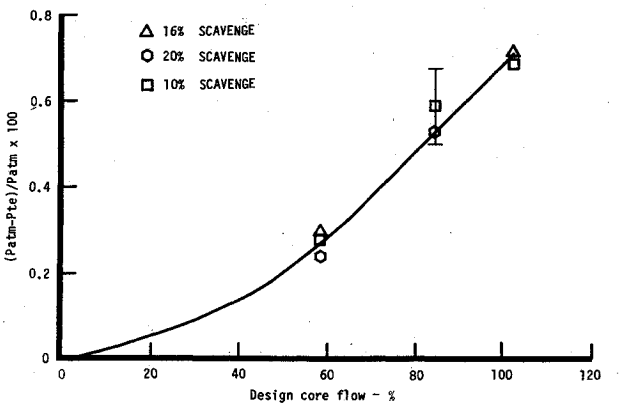

Fig. 15 Separator demonstrates low core pressure losses and low sensitivity to scavenge airflow.

the cavity above the dust, and the pressure at the seal fitting on the bottom of the hopper were separately controlled. The sand was ingested through eight tubes placed at the inlet. Sand was collected in the scavenge system through the use of Donaldson cannister-type separator/barrier filters. Separation efficiency was determined using the ratio of the weight of sand collected in the scavenge to the weight of sand ingested. A typical setup is illustrated in Fig. 13.

Results and Discussion

Good agreement was found between surface Mach numbers predicted by the flow analysis code and those calculated from experimental data (Fig. 14). As expected, deviation did occur on the shroud surface upstream of the splitter, where boundary-layer separation was predicted. The core performance was based on the mass-averaged total pressure loss from the separator entrance to the core exit. The variation of core pressure loss with core flow for different scavenge flows

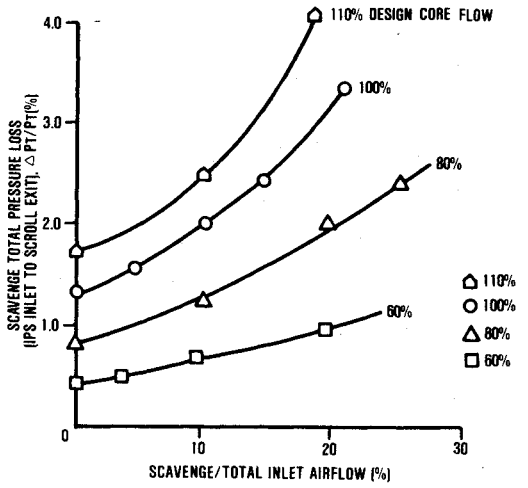

Fig. 16 Separator demonstrates low-scavenge pressure losses.

is shown in Fig. 15. The predicted total pressure loss for 15% scavenge flow was 0.7%. The scavenge system losses from the inlet to the scavenge system scroll exit are shown in Fig. 16.

Inlet distortion testing on IPS demonstrated the IPS system's ability to attenuate distortion created by severe inlet blockage. This ability is illustrated in Fig. 17. In all cases, the core flow remained dynamically stable and the distortion at the compressor inlet was reduced.

Separation tests were carried out for two types of sand particles: AC coarse dust (0-200μ) and C-spec sand (0-1000μ). Figure 18 illustrates the measured values of separation efficiency. The separator was designed to achieve a separation efficiency of 81% at 15% scavenge flow. The numerical codes underpredicted the separation efficiency for AC coarse dust.This separator demonstrated a very high separation efficiency on AC coarse dust (85%) at a scavenge flow of 16.5%.

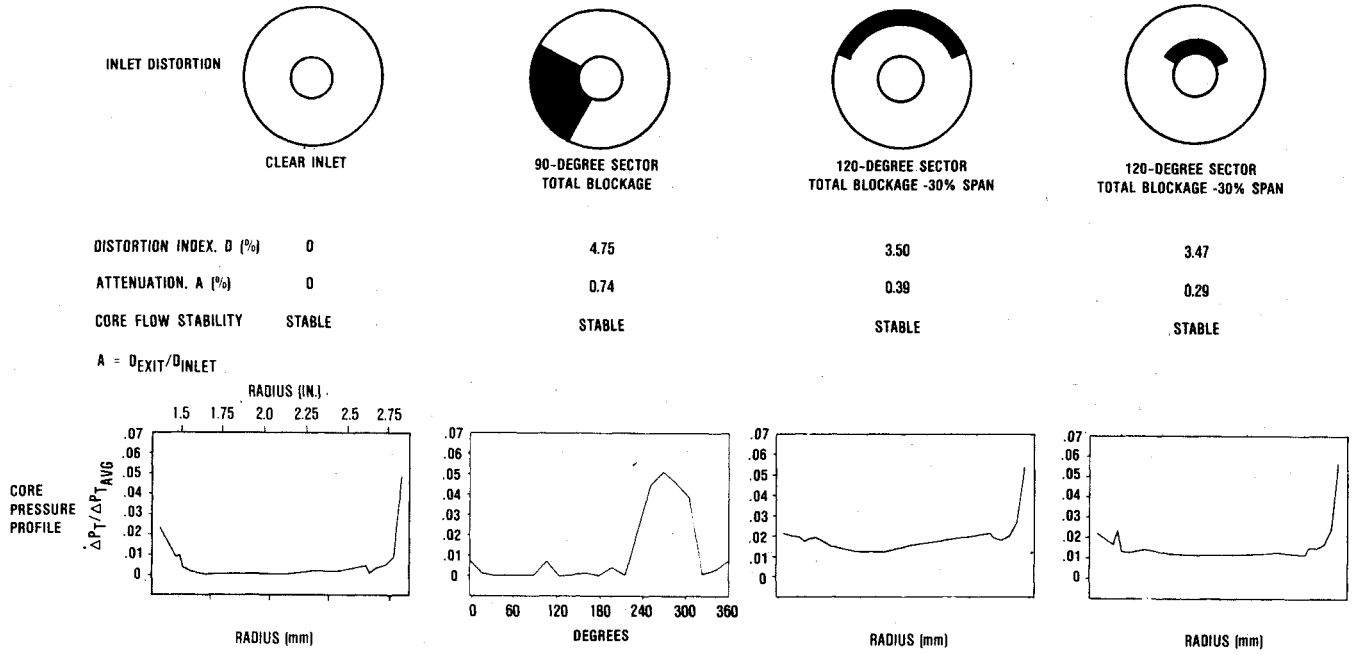

Fig. 17 Separator distortion characteristics.

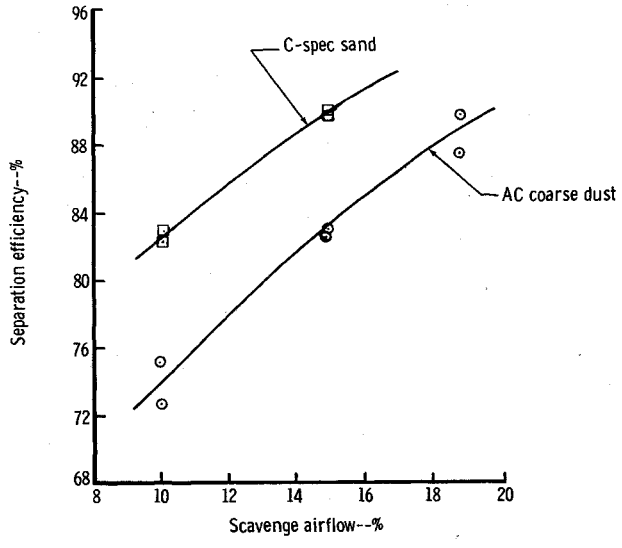

Fig. 18 Separator efficiency characteristics.

Conclusions

A building block of analytical/numerical codes has been developed and integrated to form a complete inlet particle separator design system. To validate the design system, a vaneless separator was designed and extensively tested. These tests demonstrated that a vaneless separator is able to achieve an efficiency of 85% on AC coarse dust with low total pressure loss. Weak areas in particle trajectory computation, such as rebound modeling and particle shattering, were exposed and will be addressed in the future.

Acknowledgments

The authors would like to thank Dr. A. S. Sehra, R. F. Alverson, and H. Lueders for useful discussion and A. B. Barta and S. E. Easly for test data and mechanical design, respectively.

References

[1]Shieh, C. F., Delaney, R. A., and Tipton, D. L., "Analysis of the Flow Field in an Engine Inlet Particle Separator," *Computation of Internal Flows: Methods and Applications,* ASME FED-Vol. 14, 1984.

[2]Fabian, J. H. and Oates, G. C., "Analysis of Flows within Particle Separators," ASME Paper 77-WA/FE-21, 1977.
[3]Hamed, A., "Particle Dynamics of Inlet Flow Fields with Swirling Vanes," AIAA Paper 81-0001, 1981.
[4]Katsanis, T. and Menally, W.D., "Revised Fortran Program for Calculating Velocities and Streamlines on the Hub-Shroud Mid-Channel Stream Surface of an Axial, Radial or Mixed Flow Turbomachine or Annular Duct," Vols. 1 and 2, NASA TN-D-8431, 1977.
[5]Denton, J. D., "An Improved Time Marching Method for Turbomachinery Calculation," ASME Paper 82-GT-239, 1982.
[6]McNally, W. D., "Fortran Program for Calculating Compressible Laminar and Turbulent Boundary Layer in Arbitrary Pressure Gradients," NASA TN-D5681, 1979.
[7]Shapiro, A. H., *The Dynamics and Thermodynamics of Compressible Fluid Flow*, Ronald Press Div., John Wiley & Sons, 1953.
[8]Morsi, S. A. and Alexander, A. J., "An Investigation of Particle Trajectories in Two Phase Flow Systems," *Journal of Fluid Mechanics*, Vol. 55, 1972, p. 193.
[9]Wakeman, T. J. and Takaoff, W., "Measured Particle Rebound Characteristics for Useful Erosion Prediction," ASME Paper 82-GT-170, 1982.